International Journal of Heat and Fluid Flow 30 (2009) 647–657

Contents lists available at ScienceDirect

International Journal of Heat and Fluid Flow

journal homepage: www.elsevier.com/locate/ijhff

Three-dimensional flow structure measurements behind a queue of studied model vehicles

J.F. Huang, T.L. Chan *, Y. Zhou

Department of Mechanical Engineering, The Hong Kong Polytechnic University, Hung Hom, Kowloon, Hong Kong

ARTICLE INFO

Article history:
Received 11 July 2008
Received in revised form 12 March 2009
Accepted 23 March 2009
Available online 7 May 2009

Keywords:
Wind tunnel
Particle imaging velocimetry
Vehicle wake
Flow structures

ABSTRACT

The three-dimensional flow structures of a queue of studied model vehicles (i.e., one-, two- and three-vehicle cases) were investigated comprehensively in a closed-circuit wind tunnel using particle image velocimetry (PIV) for the typical urban vehicle speeds (i.e., 10, 30 and 50 km/h). In this three-dimensional vehicle wake, a pair of longitudinal vortices is characterized by counter-rotating and moving downstream at relatively low velocity than their surrounding flow. The flow structures of multiple studied model vehicles are dominated by the wake generated from the last studied model vehicle but the preceding studied model vehicle(s) also has/have some minor effects. Cross-sectional turbulence distribution is non-uniform in the far-wake region for all studied cases. The lowest turbulence occurs at the center part of the vehicle wake while high turbulence occurs at its two sides. As such, it may lead to considerable underestimation in turbulence magnitude if the measurement is only taken along the centerline of the vehicle wake.

1. Introduction

The flow fields behind the ground vehicles play an important role in the dispersion of vehicular exhaust pollutants. The flow fields or wake structures have long been studied by researchers and engineers using different measurement techniques such as flow visualization, pressure sensor, Pitot tube, multi-hole sensor, hot wire anemometer (HWA), laser Doppler velocimetry (LDV), particle image velocimetry (PIV) etc. as well as computational fluid dynamics (CFD) techniques. More than thousands of papers and reports have been documented. So far our knowledge gained from the experimental or numerical approaches is mainly on a single ground vehicle/scale-down model vehicle either running on road or in a testing facility (e.g. wind tunnel). On the other hand, the automobile population is ever increasing in most urban cities. It leads to the growing traffic density with a shortened interval distance (i.e., vehicle spacing, safety distance etc.) between the consecutive running vehicles on the traffic lanes, and the application of modern technologies such as intelligent transport systems will further reduce the traffic/vehicle spacing (Watkins and Vino, 2008). It is clearly known that the moving ground vehicle may alter the incoming flow structures for the following vehicle(s). Here, rises a question: how much of our knowledge gained from a single moving ground vehicle can still be applied to the case among a queue of moving ground vehicles? Particular research attention has only been drawn in recent years. Up to now, very few research works concerning the flow structures, and pollutant (i.e., scalar) dispersion and concentration fields behind multiple ground vehicles have been reported.

One of the early research works concerning the vehicle queue (Clifford et al., 1997) was entirely devoted to the vehicle pollutant dispersion. They identified that 75% of the total received pollution for a following vehicle comes from the preceding one. Recently, Kanda et al. (2006a) have revealed that the pollutant dispersion in a queue of vehicles is dominated by the symmetric vehicle wake other than the offset positioned exhaust tailpipe. It can be concluded that the wake flow between vehicles moving in line affects not only their aerodynamic properties but also the vehicular exhaust pollutant dispersion patterns, if these ground vehicles are not sparsely distributed. Therefore, a better understanding of the wake region between multiple moving ground vehicles is essential.

Baker and Hargreaves (2001) and Baker (2001) stated clearly that the vehicle wakes have a significant effect on the vehicular exhaust pollutant dispersions but is over simplified by most vehicle pollutant dispersion models. He also pointed out that most of the wake studies serve for vehicle drag reduction whereas provide less attention to the interaction between the wake development and vehicular exhaust pollutant dispersion. Similar point of view has been shared by Kanda et al. (2006a) that "traffic-produced turbulence plays an important role in the dispersion of automobile exhaust gas. However, the nature of traffic-produced turbulence is poorly understood,

* Corresponding author. Tel.: +852 2766 6656; fax: +852 2365 4703.
E-mail address: mmtlchan@inet.polyu.edu.hk (T.L. Chan).

0142-727X/$ - see front matter © 2009 Elsevier Inc. All rights reserved.
doi:10.1016/j.ijheatfluidflow.2009.03.010

and the existing air pollution models adopt different empirical schemes that are difficult to verify". Consequently, they have made an assumption in their vehicle exhaust concentration test that three preceding vehicles are sufficient to produce wake turbulence equivalent to that of an infinite queue. Despite of the experimental investigations, numerical simulations also have to stem from a base weakened by the lack of knowledge about the flow around a queue of moving vehicles, "although exploratory works are emerging" (Kanda et al., 2006b). This has become a bottle neck for both experimental and numerical research works of vehicle pollutant dispersion and concentration field in a close vicinity of roadway.

In recent years, the time-averaged wake flow has been extensively studied by either traditional experimental fluid dynamics (EFD) or thriving computational fluid dynamics (CFD) methods to explain the details of aerodynamics or pollutant dispersion around the studied vehicles (Khalighi et al., 2001; Vino et al., 2003; Gosse et al., 2006a,b; Dong and Chan, 2006; Watkins and Vino, 2008; Chan et al., 2008a,b). Since the rear slant angle, $\alpha = 25^\circ$ of the present studied model vehicles is smaller than the critical angle 30°, thus it is expected a complex of three-dimensional wake will be generated (Ahmed et al., 1984; Chan et al., 2008a,b). Krajnovic and Davidson (2004) pointed out that the variety in the turbulent length scales in combination with very unsteady reattachment of separated flow in this region are possible reasons for failure of Reynolds-averaged Navier-Stokes (RANS) simulations to predict the flow around simplified car model with $\alpha = 25^\circ$ case. The hybrid LES-RANS or detached eddy simulation (DES) is still not fully developed and several problems remain to be solved for this particular rear slant angle (Krajnovic and Davidson, 2005a). The flow around Ahmed body with $\alpha = 25^\circ$ was successfully simulated using large eddy simulation (LES) (Krajnovic and Davidson, 2004, 2005a,b). Recently, Guilmineau (2008) has investigated numerically for the flow around a simplified car body with different rear slant angles (i.e., 25° and 35°) and compared with the experimental data of Lienhart and Becker (2003). He concluded that the flow around the car body with $\alpha = 25^\circ$ is still considered an open challenge for turbulence modeling. On the other hand, the EFD approaches could still provide the important flow properties for present studied model vehicles with $\alpha = 25^\circ$. The present study is to investigate the time-averaged wake flow around a queue of studied model vehicles to fill this knowledge gap. An intensive experimental investigation was performed in a well controlled wind tunnel testing facility to understand the flow structures for different vehicle queue cases because the effects of traffic vehicle movements and natural ambient wind are difficult to separate in real world. Measurement by PIV in a wind tunnel facility of the studied model vehicles will reveal the structures and properties of the air flow in wake region for one-, two- and three-vehicle cases (i.e., a queue of vehicles), especially for the scarcely research works in the latter one.

The objective of this work is to investigate three-dimensional flow structures behind a queue of studied model vehicles in a closed-circuit wind tunnel using PIV for the typical urban vehicle speeds. In the following presentation, the experimental set-up will first be described, followed by the discussions of wake structures of one-, two- and three-vehicle cases in *X*–*Y*, *X*–*Z* and *Y*–*Z* planes. Finally, some conclusions will be drawn.

2. Experimental set-up

Real on-road moving motor vehicle conditions are difficult to control, regulate and repeat. These problems bring difficulties to the induction of physical phenomena. Therefore, the present study was performed in a closed-circuit wind tunnel under a well controlled environment. The wind tunnel has a test section of $0.6 \times 0.6 \times 2$ m (Width × Height × Length). Background turbulent intensity was measured to be around 0.5% over the middle point of flat plate for a free stream velocity, $U_\infty = 8.3$ m/s. For easier comparison and continual research development, the studied model vehicles are in exactly the same shape and dimension of 1/22 scaled down model vehicle used in Chan et al. (2008a,b). All studied model vehicles (i.e., $W \times H \times L = 90 \times 81 \times 180$ mm) have a rear slant angle, $\alpha = 25^\circ$. The same studied model vehicle was used in Chan et al. (2008b) for investigating the interaction of the vehicular exhaust jet plume on flow structures, and scalar (i.e. pollutant) dispersion and concentration fields in the wake of a single studied model vehicle. The vehicular exhaust tailpipe pollutant concentration of on road vehicle was simulated using a heated air jet at certain temperature and velocity through a small tailpipe exit of 3 mm in diameter for the studied model vehicle. The vehicular exhaust tailpipe exit was located at the back side of the studied model vehicle (i.e., $X/H = 0$, $Y/H = 0.278$, $Z/H = 0.22$). Detailed geometry of this studied model vehicle(s) can be referred to Fig. 1 of Chan et al. (2008b). However, it is expected that this exhaust tailpipe exit might cause slight asymmetric flow patterns around the studied model vehicle(s) even though there was no exhaust jet flow introduced to the wake region in the present study. Blockage ratio induced by the studied model vehicle was 2%, which was well below the 5% limit suggested by Farell et al. (1977), therefore no additional blockage correction is required for the present study.

Single or multiple studied model vehicles were placed in line on a designated horizontal $2000 \times 590 \times 20$ mm ($L \times W \times Thickness$) flat plate (Chan et al., 2008b) which was supported by six supportive stands of 130 mm in height each on the bottom of test section as shown in Fig. 1. In the present study, three typical urban driving speeds of 10, 30 and 50 km/h (i.e., three free stream velocities, U_∞ of 2.78, 8.33 and 13.89 m/s in wind tunnel) were used. Their corresponding Reynolds numbers $Re_H = U_\infty \times H/\nu$ were equal to 1.48×10^4, 4.44×10^4 and 7.40×10^4, respectively. For all multiple studied model vehicle cases, the vehicle spacing between the back of the preceding vehicle and the head of the following one were fixed to allow for 2 s of the vehicle movement (i.e. vehicle spacing = $U_\infty \times 2$s). The corresponding vehicle spacing was 3.1*H*, 9.3*H* and 15.5*H* in respect to the vehicle speeds of 10, 30 and 50 km/h, as shown in Fig. 1. The origin point of Cartesian coordinate system was fixed on the ground of a designated flat plate under the center point of the back of the studied model vehicle No. 1 (hereafter referred to as V1). The *X*-axis was in the direction of main stream flow, *Y*-axis was in the direction of the width of the studied model vehicle, and *Z*-axis was in the direction of the height of the studied model vehicle. The velocity *U*, *V* and *W* are corresponded to the velocity components in *X*-, *Y*- and *Z*-directions, respectively.

One difference between the real on-road condition and wind tunnel simulation is the existence of a boundary layer over the ground for the latter case. If the 'ground' inside the wind tunnel does not move at the same speed as air flow, the boundary layer over ground will have two effects on experimental simulation: (i) the modification of the near-ground air flow structure; and (ii) the mixing of jet flow in the boundary layer (Krajnovic and Davidson 2005c). Lajos et al. (1986) compared the difference between the effects of a stationary "ground" and a moving "ground" for high-profiled vehicles (e.g. a bus) and found that the stagnation point of roll-up flow is lower for the latter case. However, Hackett et al. (1987) used a car to study the relative low-profiled vehicle and found that a moving "ground" has insignificant effects on the vehicle wake flow. Recently, Krajnovic and Davidson (2005c) have detected that the largest difference between the moving and stationary ground effects for an Ahmed body with 25° rear slant angle does not occur in the wake region behind the back of vehicle body but on the rear slant surface of the body. Similar insensitivity of vehicle wake to the ground motion was also observed by Bearman et al. (1989). Therefore, the wake flow of the studied model vehicle(s)

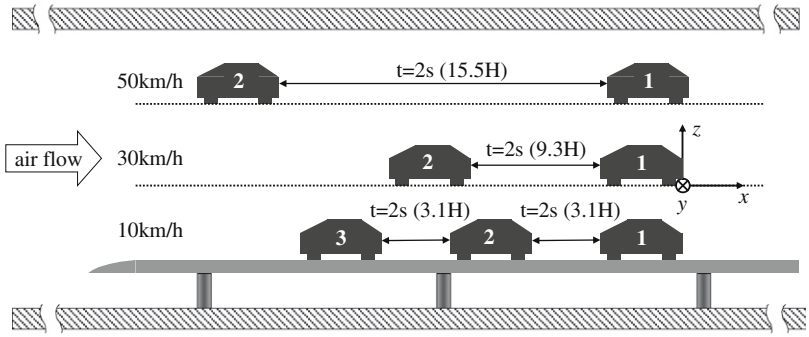

Fig. 1. Experimental setup and coordinate system inside the wind tunnel facility for one-, two- and three-vehicle cases.

with 25° rear slant angle could be considered to be insensitive to a fixed ground although the boundary layer might have a minor effect on the experimental simulation in the present study. However, the shape of the leading edge of the flat plate (Chan et al., 2008b) was designed to reduce the thickness of boundary layer by delaying the flow separation according to the research work of Narasimha and Prasad (1994). The boundary layer at the center point of the flat plate was measured by a one-dimensional hot wire probe at 8.3 m/s without placing the studied model vehicle. The thickness of boundary layer over the flat plate was measured to be less than $0.1H$ thus it is considered to be acceptable for the present study where the investigated area was up to the height of $Z = 2H$. Due to the existence of the boundary layer on the flat plate, the measured data in the close-to-ground region (i.e., $Z \leqslant 0.1H$) should be examined with certain caution because they are more or less affected by the boundary layer. For other higher regions, the measured data should not be affected.

A set of PIV from the Dantec Dynamics A/S was used to measure the flow fields in the present study. The PIV system has a dual-cavity 200 mJ Nd-YAG laser to illuminate the studied flow areas, and a double-frame HighSense4M image charge-coupled device (CCD) camera (2048 × 2048 pixels) to shoot the illuminated flow areas which were seeded by smoke particles with a mean diameter of around 0.3 μm. The captured images from the camera were stored in computer for cross-correlation analysis in order to determine the velocity vectors. A 32 × 32 pixels and 50% overlap cross-correlation arithmetic was applied to every pair of stored images to yield 127 × 127 = 16,129 vectors for the captured flow field. As the field of camera view was maintained to be $3H \times 3H$ in dimension, therefore the spatial resolution of vectors was $3H/127 = 0.024H$ (i.e., 1.9 mm for vector spacing). All investigated PIV planes were positioned either in front of or behind the last studied model vehicle (i.e. V1) as shown in Fig. 1. If there is no preceding studied model vehicle, V1 will be considered as one-vehicle case. When other studied model vehicles (only vehicle No. 2, V2 or both vehicle Nos. 2 and 3, V2 and V3) are taken into consideration by arranging one by one in the upstream, in that case V1 will be acting as the second or third vehicle in a traffic queue of multiple vehicles. For all measurements taken at the same target area, no further position adjustment of instrument is needed to cover the arrangements of these three studied vehicle queue cases (i.e., one-, two- and three-vehicle cases), therefore it would maintain a high repetition accuracy for the studied flow fields.

A one-dimensional hot wire probe was positioned behind the studied model vehicle, V1 at $X/H = 2$, $Y/H = 0$ and $Z/H = 0.5$ to measure the power spectrum of vehicle wake. Acquisition was taken to be 30 s long with a 10 kHz sampling frequency. The power spectrum curve (figure not shown) for the vehicle speed at 30 km/h (i.e., $U_\infty = 8.3$ m/s) consistently descends with the increasing of frequency and shows no obvious peak in the studied frequency range. It reveals that there is no strong periodic flow structure in the wake of the studied model vehicle. For the other two studied vehicle speeds (i.e., $U_\infty = 2.78$ and 13.89 m/s), the power spectrum curves show similar patterns. Similar results were also obtained from their studied vehicle(s) on a fixed floor by Krajnovic and Davidson (2005c) and Kanda et al. (2006a,b). This present finding confirms that the random sampling and time averaging is applicable. No phase-locked acquisition technique is required for a flow without the distinguishable periodic structures, so long as the number of random samples is large enough to obtain high averaging confidence.

The number of PIV images was then evaluated for the two-vehicle case at the vehicle speed of 10 km/h (i.e., $U_\infty = 2.78$ m/s), because the following studied model vehicle is being exposed to the highest turbulence generated by the preceding one due to the shortest vehicle spacing (i.e., $3.1H$) among all studied cases. The flow field between two studied model vehicles was selected for the evaluation purpose. A check point in the selected PIV plane was located at $1H$ upstream in the centerline of V1 and $Z = 0.5H$ above the ground of flat plate. This point was chosen because the air flow passing this selected location is an indicator for the turbulent wake of the studied model vehicle, V2 and also for the incoming flow of the studied model vehicle, V1 as shown in Fig. 2. A total of 1200 PIV images were acquired and a direct comparison was performed to show the convergence of averaged flow properties against the number of images for the selected check point as shown in Fig. 2. It can be concluded that the averaged flow properties become stable if the number of PIV images is more than 800 in the present study. Hence, the number of PIV images was chosen to

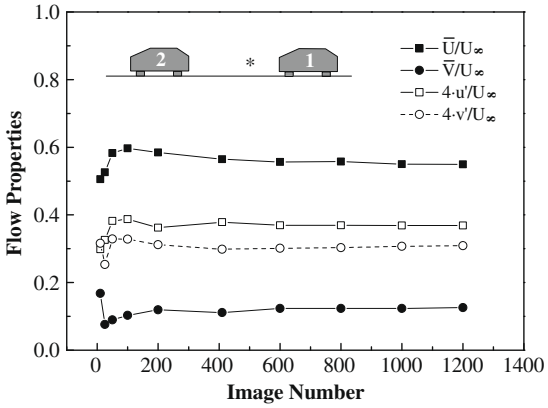

Fig. 2. Comparison of the flow properties, $\overline{U}/U_\infty, \overline{V}/U_\infty$, $4u'/U_\infty$ and $4v'/U_\infty$, from the different number of PIV images ranging from 1 to 1200 at the check point (*) at $1H$ in front of the last studied model vehicle (i.e., vehicle 1) and $0.5H$ above the ground.

be 1200 and the results were averaged from about 1080 PIV images based on a 10% rejection rate. With such number of sample images, for example the true mean velocity has 95% confidence to fall within the interval (1 ± 0.014) $\overline{U}$ or 99% confidence within (1 ± 0.019) $\overline{U}$ where $\overline{U}$ is the mean velocity using sampled PIV datasets (Benedict and Gould, 1996).

3. Results and discussion

3.1. Wake structure of one-, two- and three-vehicle cases in X–Y plane at Z/H = 0.5

3.1.1. Velocity profile for the studied model vehicles at 10 km/h

Fig. 3a and b show the cross-sectional normalized velocity, $\overline{U}/U_\infty$ and turbulence, u'/U_∞ profiles at 1H upstream from the studied model vehicle, V1 and $Z = 0.5H$ above the ground. In Fig. 3a, the profile of $\overline{U}/U_\infty$ for one-vehicle case at 10 km/h shows a shallow valley in the middle. The maximum $\overline{U}/U_\infty$ deficit is 12% due to the blockage effect from the vehicle, V1 downstream. For two-vehicle case, the curve shape is significantly altered in the wake region of the preceding studied model vehicle, V2 within $-0.9 \leqslant Y/H \leqslant 0.9$. A hill is observed in between two valleys which are caused by two counter-rotating longitudinal vortices (or trailing vortices in some literatures). At 2.1H downstream from the studied model vehicle, V2, the diameter of the vortices equals to the width of valley which is around 0.4H and the distance between two vortex centers is around 0.8H. Ahmed (1981) and Lienhart and Becker (2003) also found that the distance between two centers of longitudinal vortices is around 0.8H at the downstream 2H for their single vehicle studies. Moreover, the curve of two-vehicle case also indicates that the center part of longitudinal vortices moves along the downstream at an average velocity of $0.55U_\infty$ (i.e., the height of two curve valleys, marked by +) while the surrounding air moves at a speed of no less than $0.75U_\infty$ (i.e., the height of center hill, marked by ×). Since Fig. 3a is an averaged result of about 1080 PIV images, two possible reasons may contribute to the shape of $\overline{U}/U_\infty$ curve. One reason may be caused by the effect of statistical averaging of $\overline{U}/U_\infty$. The instantaneous $\overline{U}/U_\infty$ values inside the trailing vortices where the flow is highly turbulent may have large variation thus resulting in a lower mean value of $\overline{U}/U_\infty$ than that for the more stable outside region. Another reason is that there is not much difference between the instantaneous and averaged $\overline{U}/U_\infty$ values as shown in Fig. 3a. The $\overline{U}/U_\infty$ profiles obtained from several instantaneous vector maps (figures not shown) were examined one by one instead of using the statistical averaging approach. The results show more or less a similar curve to the one in Fig. 3a. Therefore, they justify the second reason. The longitudinal vortices are discovered to have two flow behaviors which are different from their surrounding air in vehicle wake namely counter-rotating flow as found by other researchers and moving downstream at relatively low velocity. It should be also noted that as the axis of the longitudinal vortices is in line with their downstream movement, therefore the downstream velocities for different circles of the trailing vortices are not uniform but increase with their radius from vortex center.

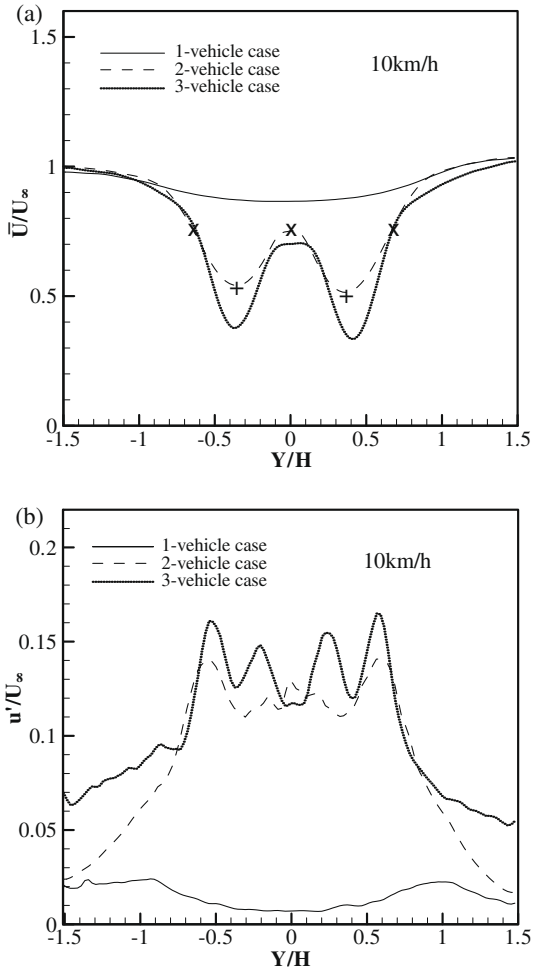

Fig. 3. Horizontal cross-sectional profiles: (a) $\overline{U}/U_\infty$, and (b) u'/U_∞ at 1H in front of vehicle 1 and $Z/H = 0.5$ above the ground for one-, two- and three-vehicle cases at 10 km/h.

The results of two- and three-vehicle cases at 10 km/h in Fig. 3a show that two preceding studied model vehicle case (i.e., both V2 and V3) has some minor changes in the wake structure or in the size of longitudinal vortices if compared with the single preceding studied model vehicle case (i.e., V2 only). Some weak effects of the expanded wake from the studied model vehicle, V3 can be observed at the two far sides of the curve. The value of mean velocity, $\overline{U}/U_\infty$ for two longitudinal vortex centers is reduced from 0.87 to 0.52 (i.e., 38% reduction) which is caused by the single blockage effect of V2 alone (i.e., two-vehicle case), and further reduction to 0.35 (i.e., 30% reduction from 0.5) by the double blockage effects of V2 and V3 (i.e., three-vehicle case). On the other hand, the value of mean turbulence, u'/U_∞ for these two longitudinal vortex centers is increased from 0.01 (i.e., background level) to 0.108 (i.e., 1070% increment) by V2 alone, and further up to 0.124 (i.e., 15% increment from 0.108) by V2 and V3.

Furthermore, as the shape of curve reflects local flow structure, the spatial coincidence of curves for two- and three-vehicle cases in Fig. 3a and b reveals that the preceding studied model vehicle, V3 does not have obvious effect on the wake structure (e.g., the position and diameter of longitudinal vortices) of the following vehicle, V2 even though the downstream movement of two longitudinal vortex centers can be considerably slowed down. It can be inferred that the wake structure behind V1 will not be significantly altered by both V2 and V3.

3.1.2. Velocity profiles for the studied model vehicles at 30 km/h

Fig. 4a and b show the cross-sectional velocity, $\overline{U}/U_\infty$ and turbulence u'/U_∞ profiles at 1H upstream from the last following studied model vehicle, V1 and $Z/H = 0.5$ for the vehicle speed at 30 km/h. In Fig. 4a, the maximum normalized mean velocity, $\overline{U}/U_\infty$ deficit is decreased from 12% (for 10 km/h case) to 5% (for 30 km/h case) due to the suppression of blockage effect by the faster incoming flow. For the two-vehicle case, the two valleys induced by the longitudinal vortices from the preceding studied model vehicle, V2 are observed to be wider and shallower if they are compared with the

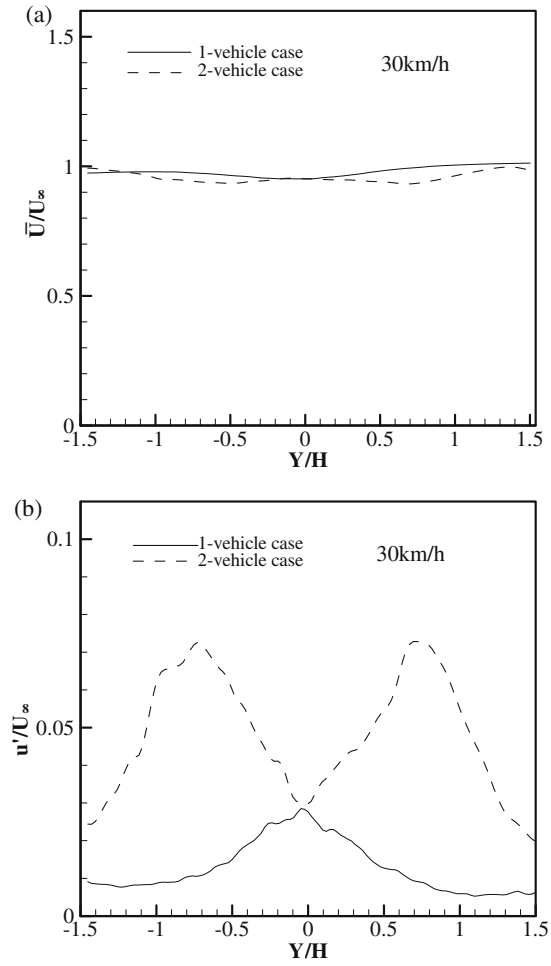

Fig. 4. Horizontal cross-sectional profiles: (a) $\overline{U}/U_\infty$, and (b) u'/U_∞ at 1H in front of vehicle 1 and $Z = 0.5H$ above the ground for one- and two-vehicle cases at 30 km/h.

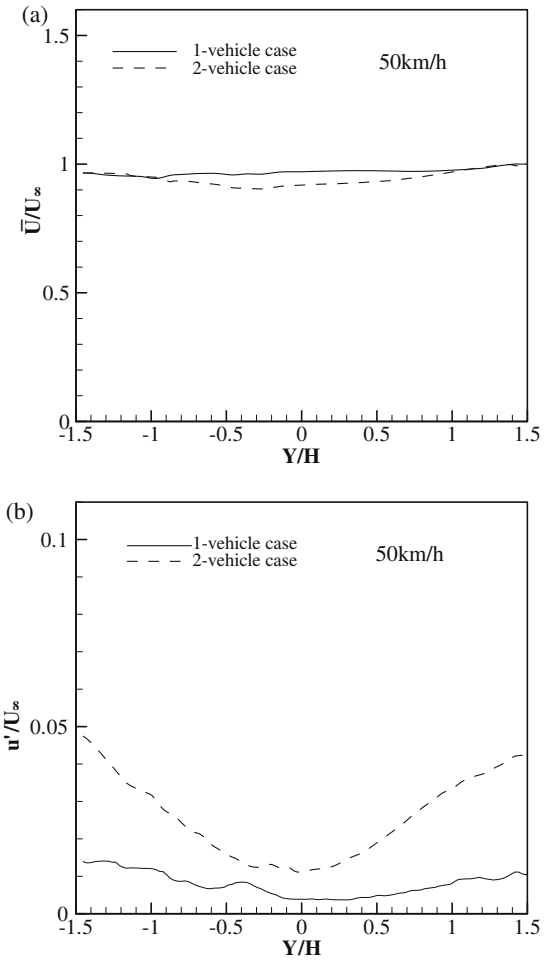

Fig. 5. Horizontal cross-sectional profiles: (a) $\overline{U}/U_\infty$ and (b) u'/U_∞ at 1H in front of vehicle 1 and $Z = 0.5H$ above the ground for one- and two-vehicle cases at 50 km/h.

valleys for two-vehicle case at 10 km/h. It might be because the vehicle spacing has been increased from 3.1H to 9.3H. According to the description of Baker (2001), the near-wake region is characterized by the large-scale flow structures from 0 to 10H behind the vehicle, and the far-wake region is characterized by the gradual decay beyond 10H. Supported by the Baker's conclusion and eddy energy cascade theory, it is believed that the two wide and shallow valleys are not induced by the weak longitudinal vortices but by many small-scaled eddies broken from the longitudinal vortices. Several $\overline{U}/U_\infty$ curves from the instantaneous vector maps (figures not shown) were checked. Each curve has a few valleys which are small, shallow and almost randomly positioned. None of these checked curves show a symmetric pattern or any valley as wide as these two valleys in Fig. 4a. Therefore, it can be concluded that contrary to the case of 10 km/h, the two shallow valleys in the $\overline{U}/U_\infty$ curve for 30 km/h are the averaging effect of many small sized eddies, and the two longitudinal vortices of 0.4H in diameter have already been broken apart along the way between $X/H = 2.1$ and 8.3. In Fig. 4b, the distance between two averaged valley centers can be more accurately determined from the two peaks in the curve of u'/U_∞ to be about 1.5H at $X/H = 8.3$, in contrast to the about 0.8H at $X/H = 2.1$ in Section 3.1.1.

3.1.3. Velocity profile for the studied model vehicles at 50 km/h

Fig. 5a and b show the cross-sectional velocity, $\overline{U}/U_\infty$ and turbulence u'/U_∞ profiles at 1H upstream from the last following studied model vehicle, V1 and $Z/H = 0.5$ for the vehicle speed at 50 km/h. The difference between the curves of $\overline{U}/U_\infty$ and u'/U with and without a preceding studied model vehicle are both within 5%. No large flow structure can be found in the far-wake region at 14.5H and $Z/H = 0.5$ behind the preceding studied model vehicle, V2 for two-vehicle case. Interestingly the center part of vehicle wake has the lowest turbulence intensity which is close to background level, in sharp contrast to the preceding studied model vehicle cases at 10 km/h. It can be inferred that the difference in incoming flow caused by the preceding vehicle on the following vehicle, V1 can be ignored in most engineering applications if the vehicle separation is larger than 15H, because the difference in flow properties of $\overline{U}/U_\infty$ and u'/U_∞ is less than 5% when comparing the preceding vehicle with no preceding vehicle case.

An unexpected phenomenon is observed in the present study. The turbulence, u'/U_∞ profile in Fig. 5b is still quite non-uniform even in the far-wake region, 14.5H downstream from the preceding studied model vehicle, V2. The lowest turbulence, $u'/U_\infty = 0.012$ still occurs at the center part of wake while the highest turbulence, $u'/U_\infty = 0.048$ occurs at the two far sides. Such high turbulence is believed to be induced by the broken eddies from the trailing vortices. Comparing with the turbulence, u'/U_∞ profiles at $X/H = 8.3$ and $X/H = 14.5$ in Figs. 4b and 5b, it can be observed that from the near-wake region to the far-wake region of the studied model vehicles, the turbulence in wake decreases for the whole cross-section profile, but the width of turbulent wake in the Y-direction has considerably expanded along the downstream distance.

3.1.4. Streamwise velocity $\overline{U}/U_\infty$ and momentum $u'v'/U^2_\infty$ contours for the studied model vehicles at different vehicle speeds

Fig. 6 shows the contours of $\overline{U}/U_\infty$ in X–Y plane at $Z/H = 0.5$ behind the last studied model vehicle, V1 for one-vehicle case at 10 km/h. Two "hills" occur shortly behind the vehicle back (i.e., $X/H \approx 0.3$), and then they converge to form a "ridge" at $X/H \approx 1$. The height of hill does not change with the addition of preceding studied model vehicles but the height of ridge does. The heights of hill and ridge are (0.30, 0.78) for one-vehicle case and (0.30, 0.82) for two-vehicle case and (0.30, 0.85) for three-vehicle cases. For other two vehicle speeds (i.e., 30 and 50 km/h), their contours (figures not shown) are similar in shape but different in values. Their heights of hill and ridge are (0.39, 0.86) for one-vehicle case and (0.43, 0.94) for two-vehicle case at 30 km/h, or (0.45, 0.91) for one-vehicle case and (0.48, 0.97) for two-vehicle case at 50 km/h, respectively.

In Fig. 6, the most noticeable difference induced by preceding studied model vehicles is the height of 'ridge', 0.78, 0.82 and 0.85 for one- two- and three-vehicle cases at 10 km/h, respectively. It should be noted that the height of $\overline{U}/U_\infty$ rises with the increasing upstream blockage. An explanation can be referred to the vorticity contours of Fig. 11. The absolute vorticity value (i.e., the changing rate of movement direction) over the rear slant of V1 will be decreased from 12.1 to 9.9 or 9.8 if one or two preceding studied model vehicle(s) is/are arranged in the upstream of V1, thus resulting in less downwashing flow over the rear slant and producing a higher $\overline{U}/U_\infty$ value in the near-wake region. This phenomenon may also explain why the $\overline{U}/U_\infty$ values are increased by a preceding vehicle from 0.86 to 0.94 and 0.91 to 0.97 for 30 km/h and 50 km/h cases, respectively.

Watkins and Vino (2008) have recently found that the relationship between the vehicle spacing and aerodynamics that both lift and drag coefficients vary remarkably within the vehicle spacing ranging from 0.1 to 1.0L ($1L = 3.6H$). Beyond a turning point at 1.0L, both studied coefficients become relatively stable especially for the drag which is maintained at 88% of their values for one-vehicle case. Fig. 6 shows that the flow properties such as $\overline{U}/U_\infty$ in very near-wake region (i.e., $X/H \leqslant 1$) change drastically with downstream distance. Beyond this very near-wake region where the 'ridge' is formed, both the shape and values of $\overline{U}/U_\infty$ become stable. It can be inferred that the resulting aerodynamics forces will follow similar trend of the flow properties.

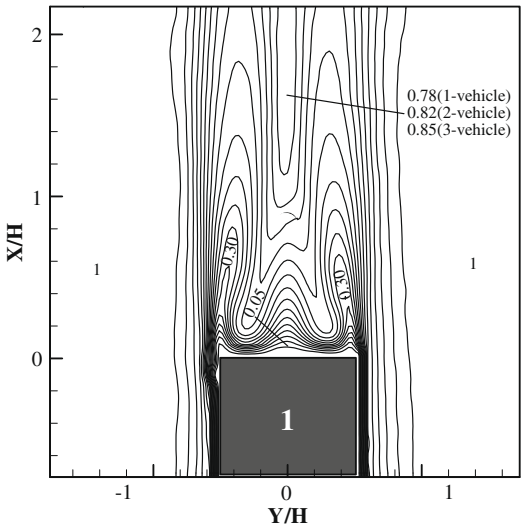

Fig. 6. Contours of $\overline{U}/U_\infty$ in X–Y plane at $Z/H = 0.5$ for one-, two- and three-vehicle cases at 10 km/h (Contour base line = 0.005, step = 0.005).

Because turbulence plays an important role in mixing processes including the pollutant dispersion and concentration field of moving vehicle(s) in atmosphere, the averaged turbulent stress, $|\overline{u'v'}|/U^2_\infty$ contours in X–Y plane are shown in Fig. 7a–c for one-vehicle cases at 10, 30 and 50 km/h, respectively. In Fig. 7a, two peaks of $|\overline{u'v'}|/U^2_\infty$ with the height around 0.0134 can be observed at $X/H = 0.6$ and $Y/H = \pm 0.45$. One or two preceding studied model vehicles may not obviously change the structure of $|\overline{u'v'}|/U^2_\infty$ behind the vehicle V1 because the peak values always occur around 0.5–0.6H regardless of the presence of preceding vehicle(s) (figures not shown). The peak values of $|\overline{u'v'}|/U^2_\infty$ are raised up to 0.0147 by V2 alone or 0.0155 by both V2 and V3. Similar $|\overline{u'v'}|/U^2_\infty$ contours are also observed for the vehicle speed of 30 km/h and 50 km/h.. For the one-vehicle case (i.e. V1 only) at three different vehicle speeds as shown in Fig. 7a–c, it can be concluded that the $|\overline{u'v'}|/U^2_\infty$ values increase with increasing vehicle speed. Furthermore, the preceding studied model vehicle, V2 may increase the $|\overline{u'v'}|/U^2_\infty$ values by 17% for 30 km/h case or 13% for 50 km/h case (figures not shown). On the other hand, V2 only increases the turbulent intensity, u'/U_∞ value by 6% for 30 km/h or 2% for 50 km/h. Clearly, the preceding vehicle has more effect on $|\overline{u'v'}|/U^2_\infty$ than on u'/U_∞. The distribution pattern of $|\overline{u'v'}|/U^2_\infty$, is not sensitive to either the vehicle speed or the presence of preceding vehicle(s).

3.2. Wake structure in X–Z plane at Y/H = 0

Normalized $\overline{U}/U_\infty$ and u'/U_∞ profiles along the Z-direction at 1H in front of the head of the studied model vehicle, V1 for one-, two- and three- vehicle cases at 10 km/h are shown in Fig. 8a and b. The preceding studied model vehicle, V2 of two-vehicle case may decrease $\overline{U}/U_\infty$ by 15% and increase u'/U_∞ by 8% at most for the incoming flow to the following vehicle, V1. The blockage effect of V2 is obvious for the flow region lower than $Z/H = 1$ but still noticeable at $Z/H = 2$. It can be concluded that for the difference in flow properties of $\overline{U}/U_\infty$ and u'/U_∞ induced by both preceding studied model vehicles, V2 and V3, the blockage effect of V2 contributes more than 90% of the difference in the flow properties while the blockage of V3 has just a minor effect for less than 10%. This phenomenon in the X–Z plane is similar to that in X–Y plane as mentioned in Section 3.1. In Figs. 9a and 10a for one- and two-vehicle cases at 30 and 50 km/h, the blockage effect of preceding model vehicle, V2 on $\overline{U}/U_\infty$ is weakened by 50% or more because of the larger vehicle spacing for wake development. The values of u'/U_∞ induced by the presence of V2 are around 5% for both 30 km/h and 50 km/h cases as shown in Figs. 9b and 10b.

Fig. 11a–c show the normalized vorticity, $\overline{\omega}_y \cdot H/U_\infty$ in X–Z plane for one-, two- and three- vehicle cases at 10 km/h, respectively. Again the preceding studied model vehicle, V2 makes a more noticeable difference in the value of vorticity than in structure. Peak vorticity values are changed from $(-12.1, 7.5)$ to $(-9.8, 7.0)$ by V2. But the second preceding studied model vehicle, V3 has almost no effect on the vorticity value over the rear slant of V1. Its effect on the positive signed vortex in the lower part of the wake region is still discernible. The peak vorticity values for the three preceding vehicle cases are $(-9.9, 6.7)$. It can be concluded that the two preceding vehicles change the lower part of the wake region more severely than the upper part. The normalized circulation values of positive signed vortex structure, $\overline{\Gamma}_y/(U_\infty \cdot H)$ are 2.5, 2.1 and 2.0 for one-vehicle, two-vehicle and three-vehicle cases at 10 km/h, respectively (i.e. 16% reduction by V2 alone or 36% reduction by both V2 and V3). The changes in circulation values caused by the preceding vehicles are more prominent than in the peak vorticity values because the vortex sizes are also decreased.

The extension of separation bubble, X_{NW} was previously reported to be 0.65H by experiment (Lienhart and Becker, 2003) or by LES (Krajnovic and Davidson, 2005a). The flow structure in

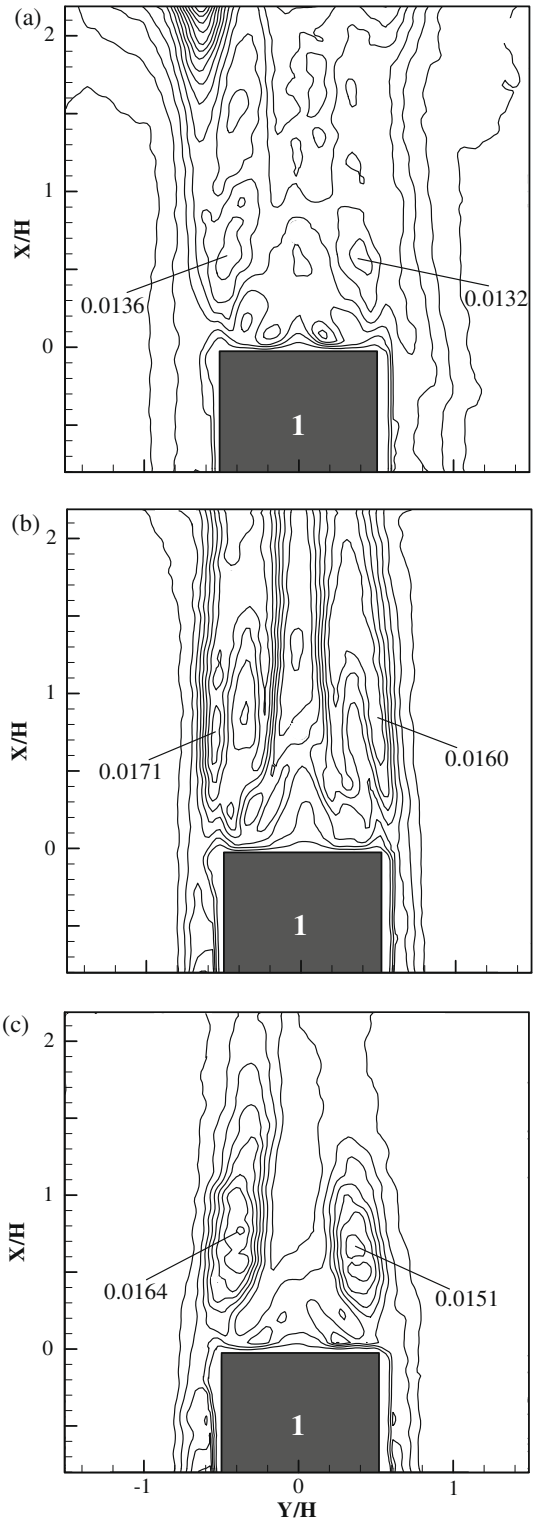

Fig. 7. Averaged turbulent stress, $|\overline{u'v'}|/U_\infty^2$ contours in X–Y plane at $Z/H = 0.5$ for one-vehicle case at: (a) 10 km/h, (b) 30 km/h and (c) 50 km/h (Contour base line = 0.002, step = 0.002).

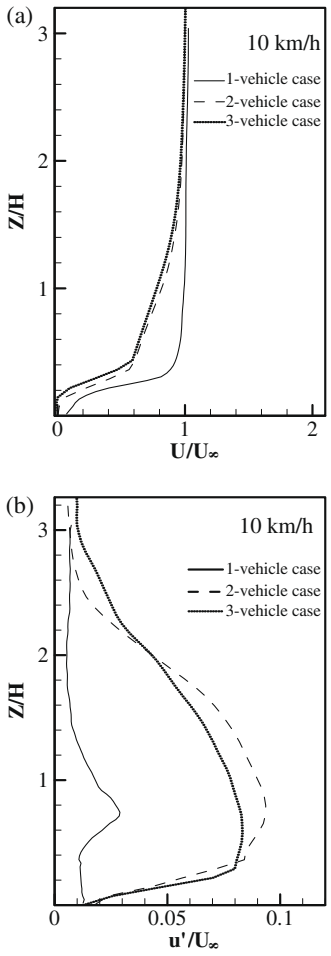

Fig. 8. (a) $\overline{U}/U_\infty$, and (b) u'/U_∞ profile in X–Z plane at $1H$ in front the head of last studied model vehicle (i.e., vehicle 1) for one-, two- and three-vehicle cases at 10 km/h.

Fig. 11a shows that $X_{NW,}$ is around $0.64H$ for 10 km/h and remains the same for up to 50 km/h in Fig. 12 for the present study. The results presented good agreement with the experimental and numerical results obtained from Lienhart and Becker (2003) and Krajnovic and Davidson (2005a), respectively for single vehicle case. Fig. 11a also justifies the removal of a small vortex generated by inadequate resolution in coarse and medium grid using LES approach (Krajnovic and Davidson 2005a). Krajnovic and Davidson (2005a) assumed that "the Reynolds number and resolution requirements could be decreased if the positions of the recirculating regions in the flow are defined by the geometry rather than by the viscosity and upstream conditions". In the present study, the values of X_{NW} remain constant from 10 to 50 km/h as shown in Figs. 11a and 12, and justify their assumption for single vehicle case. However, the values of X_{NW} will decrease with increasing number of the preceding studied model vehicle(s) in a queue arrangement (e.g., $0.64H$, $0.54H$ and $0.52H$ for one-, two- and three-vehicle cases at 10 km/h, respectively as shown in Fig. 11a–c, $0.64H$ and $0.61H$ at 30 km/h (figures not shown), or $0.64H$ and $0.62H$ at 50 km/h (figures not shown) for one- and two-vehicle cases, respectively). This length shrinkage of X_{NW} might be caused by the reducing blockage effect of preceding vehicle(s) in respect to the height from ground as shown in Figs. 8a, 9a and 10a.

At higher vehicle speed of 30 km/h or 50 km/h, the preceding studied model vehicle, V2 may reduce the peak vorticity values of $\overline{\omega}_y \cdot H/U_\infty$ from $(-9.1, 8.2)$ to $(-9.0, 7.1)$ or $(-9.0, 8.6)$ to $(-8.9, 6.0)$, respectively (figures not shown). The corresponding normalized circulation values $\overline{\Gamma}_y/(U_\infty \cdot H)$ for positive signed vortex structure are also reduced from 3.5 to 3.0 (i.e., 14% reduction) or from 3.1 to 2.3 (i.e., 25% reduction), respectively (figures not shown). The changes induced by the preceding vehicle in the $\overline{\omega}_y \cdot H/U_\infty$ contours for these two vehicle speeds are less obvious

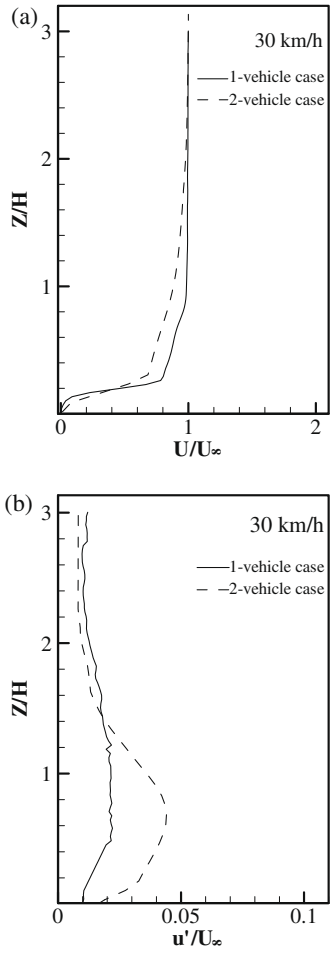

Fig. 9. (a) $\overline{U}/U_\infty$ and (b) u'/U_∞ profile at $1H$ in front of the head of the last studied model vehicle (i.e., vehicle 1) for one- and two-vehicle cases at 30 km/h.

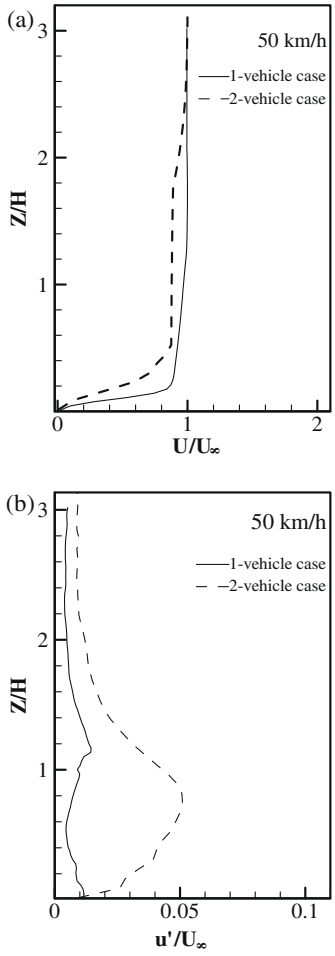

Fig. 10. (a) $\overline{U}/U_\infty$ and (b) u'/U_∞ profile in X–Z plane at $1H$ in front of the head of the last studied model vehicle (i.e., vehicle 1) for one- and two-vehicle cases at 50 km/h.

than for 10 km/h while the positively signed recirculation zone still shows higher sensitivity than other negatively signed parts.

The Reynolds shear stress, $\overline{u'w'}/U_\infty^2$ contours for one-, two and three-vehicle cases at 10 km/h are shown in Fig. 13a–c. The peak values of $\overline{u'w'}/U_\infty^2$ in the lower wake region consistently decrease from 0.025 to 0.015 and further to 0.011 with the addition of preceding vehicles, while the values of $\overline{u'w'}/U_\infty^2$ over the surface of rear slant back remains 0.020 regardless of the presence of preceding vehicle(s). It should be noted that the occurrence positions of this peak value of $\overline{u'w'}/U_\infty^2$ for 0.020 get much closer to the surface of rear slant back and the pattern of contour lines on top is significantly altered by the preceding vehicle(s). As the exhaust tailpipe of vehicle is often positioned in the lower part of the studied vehicle back, it can be inferred that preceding vehicles may have considerable effect on the vehicular exhaust pollutant dispersion by decreasing $\overline{u'w'}/U_\infty^2$ for 40% or more. More research work is deserved for the lower wake region. Due to space limitation, the contours of $\overline{u'w'}/U_\infty^2$ for 30 and 50 km/h cases are not shown here. The preceding studied model vehicle, V2 also reduces the peak values of Reynolds shear stress $\overline{u'w'}/U_\infty^2$ from $(0.030, 0.034)$ to $(0.034, 0.028)$ or from $(0.023, 0.027)$ to $(0.036, 0.025)$ for 30 and 50 km/h, respectively, in the wake of vehicle, V1. The changes in $\overline{u'w'}/U_\infty^2$ values and patterns induced by the preceding vehicles decrease with increasing vehicle spacing. It should be noted that the values of $\overline{u'w'}/U_\infty^2$ are prominently weakened by the preceding vehicles while in contrast the values of $\overline{u'v'}/U_\infty^2$ are strengthened.

3.3. Wake structure in Y–Z planes

3.3.1. Vorticity contours in Y–Z plane at X/H = 1 for the studied model vehicles at different vehicle speeds

Normalized streamwise vorticity, $\overline{\omega}_x \cdot H/U_\infty$ contours in Y–Z plane at $X/H = 1$ for one-vehicle case at 10, 30 and 50 km/h are shown in Fig. 14a–c. The flow patterns show good agreement with the results obtained from the EFD by Kozaka et al. (2004) and CFD by Chan et al. (2008a). A pair of counter-rotating vortices is distributed at $Y/H = \pm 0.25$ and $Z/H = 0.65$ with the maximum vorticity, $\overline{\omega}_x \cdot H/U_\infty$ values $(-2.35, 2.77)$. The preceding studied model vehicle, V2 at $3.1H$ upstream from the following studied model vehicle, V1 has no noticeable effect on the pattern of $\overline{\omega}_x \cdot H/U_\infty$ contours, but reduces its maximum vorticity values to $(-2.00, 2.22)$. The second preceding vehicle, V3 still has no prominent effect on the contour pattern, though it can further reduce the maximum vorticity to $(-1.91, 2.16)$. The corresponding normalized circulation values $\overline{\Gamma}_x/(U_\infty \cdot H)$ for the three preceding cases are 3.9, 3.7 and 3.5, respectively (i.e. 4% reduction by the preceding vehicle V2 alone or 10% reduction by both V2 and V3). Therefore, it can be concluded that the presence of the preceding vehicles does not have much effect on the wake structure of V1 but has more obvious effect on the values of vorticity and circulation in the Y–Z plane, as in the other two planes (i.e., X–Y and X–Z). Contrary to the results of 10 km/h in X–Z plane, the effect of preceding vehicles is more prominent in peak vorticity than in circulation values in Y–Z plane.

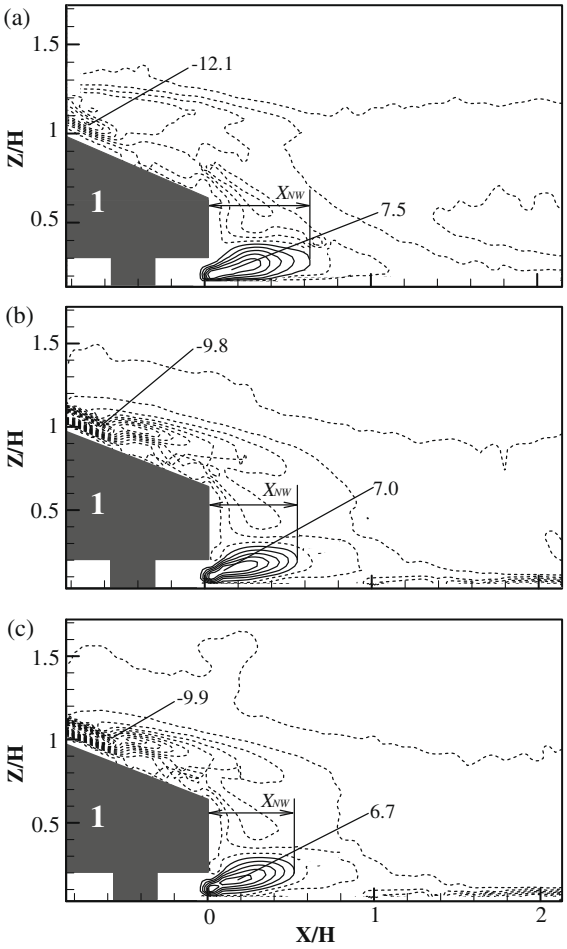

Fig. 11. Vorticity, $\overline{\omega}_y \cdot H/U_\infty$ contours in X–Z plane for: (a) one-vehicle, (b) two-vehicle, and (c) three-vehicle cases at 10 km/h (Contour base line = 1, step = 1).

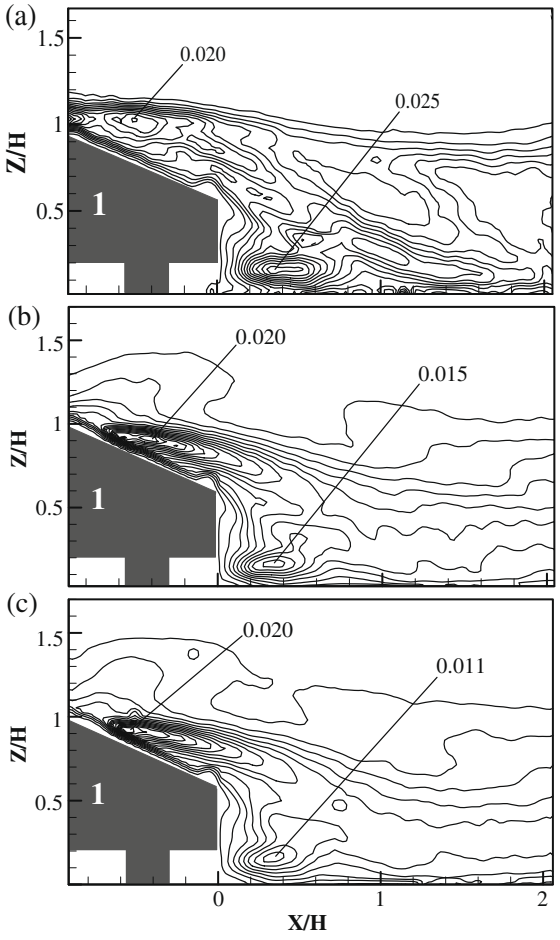

Fig. 13. Reynolds shear stress, $|\overline{u'w'}|/U_\infty^2$ contours in X–Z plane for: (a) one-vehicle, (b) two-vehicle, and (c) three-vehicle cases at 10 km/h (Contour base line = 0.0025, step = 0.0025).

In addition to the 10 km/h case, the pattern of $\overline{\omega}_x \cdot H/U_\infty$ is also observed to be independent of the preceding vehicle, V2 for 30 km/h and 50 km/h cases by comparing the contours of $\overline{\omega}_x \cdot H/U_\infty$ with and without V2 cases (contours of $\overline{\omega}_x \cdot H/U_\infty$ with V2 not shown). The effect of the preceding vehicle, V2 is also more obvious in vorticity values than in wake structure of V1. For 30 km/h case, the preceding vehicle, V2 reduces the maximum vorticity value $\overline{\omega}_x \cdot H/U_\infty$ of the following model vehicle, V1 from $(-2.75, 3.16)$ to $(-2.29, 2.34)$ (i.e. 22% reduction) and the normalized circulation value $\overline{\Gamma}_x/(U_\infty \cdot H)$ from 3.9 to 3.4 (i.e. 13% reduction). For 50 km/h case, the preceding studied model vehicle, V2 reduces the maximum vorticity value of the following studied model vehicle, V1 from $(-2.74, 3.14)$ to $(-2.21, 2.61)$ (i.e. 18% reduction) and the normalized circulation value $\overline{\Gamma}_x/(U_\infty \cdot H)$ from 4.0 to 3.5 (i.e. 14% reduction). It should be noted that the vehicle spacing is almost three times (i.e, for 30 km/h) or five times (i.e., for 50 km/h) long if compared with that of 10 km/h case. However, the reduction in maximum vorticity value of the following vehicle, V1 induced by the preceding vehicle(s) (i.e, V2 only or both V2 and V3) is still comparable to the 10 km/h case (around 17% reduction). It reveals that the decreasing effect of preceding vehicle on the vorticity of trailing vortices from a following vehicle is insensitive to the vehicle spacing. Watkins and Vino (2008) have also recently presented similar findings for the relationship between the vehicle spacing and drag force. The curve of drag coefficient for the following studied model vehicle is almost parallel to that for an isolated vehicle regardless of the large vehicle spacing (i.e., $X/L \geqslant 1$ or $X/H \geqslant 3.6$).

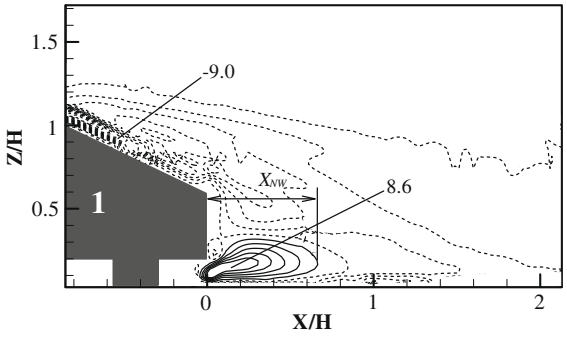

Fig. 12. Vorticity, $\overline{\omega}_y \cdot H/U_\infty$ contours in X–Z plane for one-vehicle case at 50 km/h (Contour base line = 1, step = 1).

3.3.2. Vorticity contours in Y–Z plane at X/H = 3 for the studied model vehicles at different vehicle speeds

Normalized streamwise vorticity, $\overline{\omega}_x \cdot H/U_\infty$ contours in Y–Z plane at $X/H = 3$ for one-vehicle case at 10, 30 and 50 km/h are shown in Fig. 15a–c. Because downwash flow is the main stream in the near-wake region of the studied model vehicle at $X/H = 3$, it pushes the longitudinal vortices closer to the ground if compared with the Fig. 14 at $X/H = 1$. The maximum $\overline{\omega}_x \cdot H/U_\infty$ values of the trailing vortices for one-vehicle case at 10 km/h are $(-2.35, 2.77)$ at $X/H = 1$, $(-1.90, 1.94)$ at $X/H = 2$ (figures not shown) and

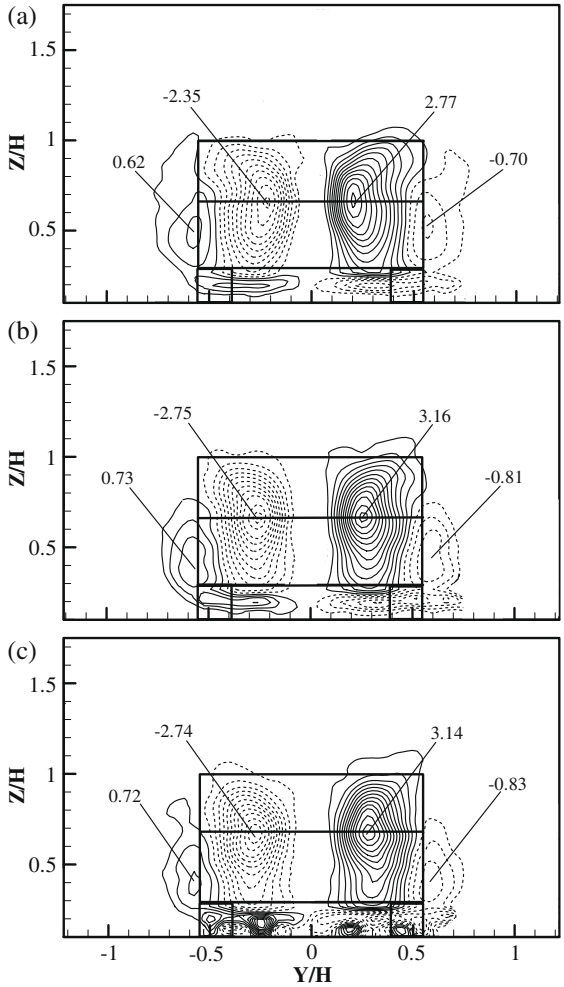

Fig. 14. Vorticity, $\overline{\omega}_x \cdot H/U_\infty$ contours in Y–Z plane at $X/H = 1$ for one-vehicle case at: (a) 10 km/h, (b) 30 km/h, and (c) 50 km/h (Contour base line = 0.2, step = 0.2).

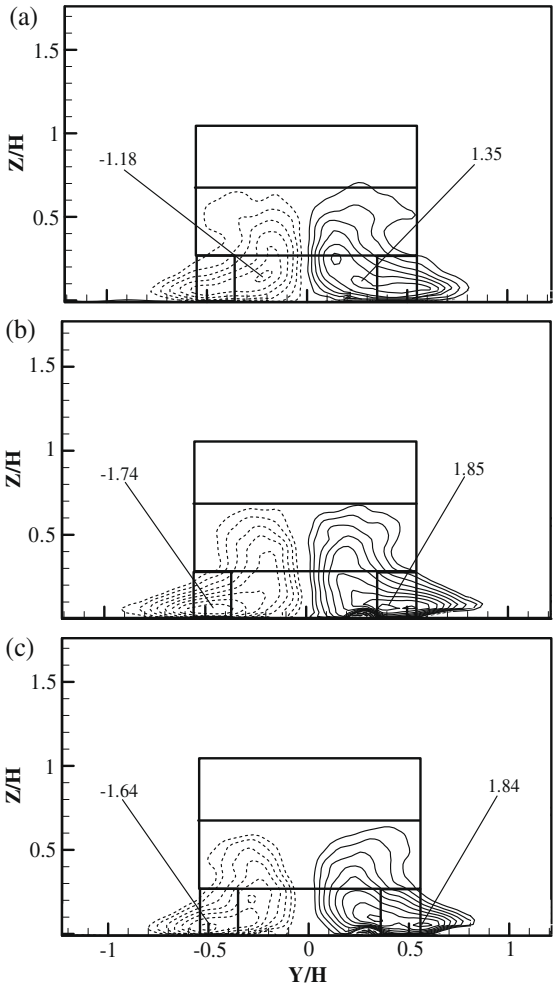

Fig. 15. Vorticity, $\overline{\omega}_x \cdot H/U_\infty$ contours in Y–Z plane at $X/H = 3$ for one-vehicle case at: (a) 10 km/h, (b) 30 km/h, and (c) 50 km/h (Contour base line = 0.2, step = 0.2).

$(-1.18, 1.35)$ at $X/H = 3$. At $X/H = 3$, the presence of the preceding vehicle(s) cannot induce any obvious effect in the wake structure, as happened at $X/H = 1$. However, the reduction in vorticity values induced by the preceding vehicle(s) is/are still noticeable. The maximum $\overline{\omega}_x \cdot H/U_\infty$ values of the trailing vortices from the vehicle, V1 are reduced from $(-1.18, 1.35)$ to $(-1.09, 1.21)$ (i.e., 9% reduction) by the preceding vehicle, V2 only or reduced from $(-1.18, 1.35)$ to $(-0.95, 1.12)$ (i.e., 19% reduction) by both preceding vehicles, V2 and V3. The corresponding normalized circulation values $\overline{\Gamma}_x/(U_\infty \cdot H)$ for these three preceding cases are 2.9, 2.6 and 2.0, respectively (i.e. 10% reduction by V2 alone or 31% reduction by both V2 and V3).

The presence of the preceding vehicle, V2 for the 30 and 50 km/h cases still cannot induce any obvious effect in the wake structure at $X/H = 3$ but produces some differences in vorticity values. Therefore, only vorticity contours for one-vehicle cases at these two vehicle speeds are shown in Fig. 15b and c, respectively. The maximum vorticity values $\overline{\omega}_x \cdot H/U_\infty$ of the trailing vortices from the studied model vehicle, V1 are reduced from $(-1.74, 1.85)$ to $(-1.52, 1.82)$ (i.e., 7% reduction) for 30 km/h or reduced from $(-1.64, 1.84)$ to $(-1.66, 1.81)$ (i.e., 0.3% reduction) for 50 km/h caused by the preceding vehicle, V2. The normalized circulation values $\overline{\Gamma}_x/(U_\infty \cdot H)$ of trailing vortices are reduced by V2 alone from 3.8 to 3.7 (i.e. 3% reduction) for 30 km/h and 4.2 to 3.9 (i.e. 9% reduction) for 50 km/h, respectively.

Table 1
Average longitudinal peak vorticity behind the last studied model vehicle for different vehicle speeds and arrangements of preceding studied model vehicle(s).

Vehicle speed	Number of preceding vehicle(s)	$X/H = 1$	$X/H = 2$	$X/H = 3$
10 km/h	0	2.56	1.92	1.27
	1	2.11	1.50	1.25
	2	2.04	1.28	1.04
30 km/h	0	2.96	2.07	1.80
	1	2.31	1.86	1.67
50 km/h	0	2.94	2.08	1.74
	1	2.41	1.83	1.73

3.4. Summary for the characteristics of maximum vorticity values for trailing vortices at different X/H locations and vehicle speeds for one-, two- and three-vehicle cases

Longitudinal peak vorticity values measured behind the last studied model vehicle, V1 for different vehicle speeds and arrangements of preceding studied model vehicle(s) are summarized in Table 1.

4. Conclusions

The three-dimensional flow structures of a queue of studied model vehicles (i.e., one-, two- and three-vehicle cases) were investigated comprehensively in a closed-circuit wind tunnel using

particle image velocimetry (PIV) for the typical urban vehicle speeds (i.e., 10, 30 and 50 km/h).

The longitudinal vortices are found to be counter-rotating and moving downstream at relatively low velocity if compared with their surrounding flow. Inside the longitudinal vortices, there are velocity gradients along the vortex radius for the downstream movement, and the lowest downstream velocity occurs at vortex cores. The velocity difference is up to $0.25U_\infty$ between the center and edge of longitudinal vortices.

The wake flow structure of a vehicle queue is mainly dominated by its immediate upstream vehicle rather than the incoming flow altered by the preceding studied model vehicle(s). While the downstream vehicle has the most pronounced effect on the wake flow structure, all the upstream model vehicle(s) still has/have some effects. The changes induced by the upstream vehicles in wake flow structure are often within the order of 10%, and at an order of 20% in flow properties (e.g., mean and turbulent velocity, vorticity, shear stress etc). In the present study, it was observed that the mean and turbulent velocities are more sensitive to vehicle spacing than the shear stress and vorticity.

Cross-sectional turbulence distribution is still non-uniform in the far-wake region. The low turbulence occurs at the center part of the wake flow while the high turbulence occurs at its two sides. For such a turbulence distribution, it may lead to considerable underestimation on turbulence magnitude if the measurement is only taken along the centerline of the vehicle wake.

Acknowledgements

This work was supported by the grants from the Central Research Grants and the research studentship of The Hong Kong Polytechnic University, Hong Kong.

References

Ahmed, S.R., 1981. Wake structure of typical automobile shapes. J. Fluid Eng. 103, 162–169.

Ahmed, S.R., Ramm, G., Faltin, G., 1984. Some salient features of the time-averaged ground vehicle wake. SAE Technical Paper 840300.

Baker, C.J., Hargreaves, D.M., 2001. Wind tunnel evaluation of a vehicle pollution dispersion model. J. Wind Eng. Ind. Aerod. 89 (2), 187–200.

Baker, C.J., 2001. Flow and dispersion in ground vehicle wakes. J. Fluid Struct. 15 (7), 1031–1060.

Bearman, P.W., De Beer, D., Hamidy, E., Harvey, J.K., 1989. The effect of a moving floor on wind tunnel simulation of road vehicles. SAE Technical Paper 880245.

Benedict, L.H., Gould, R.D., 1996. Towards better uncertainty for turbulence statistics. Exp. Fluid 22 (2), 129–136.

Chan, T.L., Luo, D.D., Cheung, C.S., Chan, C.K., 2008a. Large eddy simulation of flow structures and pollutant dispersion in the near-wake region of the studied ground vehicle for different driving conditions. Atmos. Environ. 42 (21), 5317–5339.

Chan, T.L., Gosse, K., Zhou, Y., Lee, S.C., Wang, X.W., Huang, J.F., 2008b. Effect of rear slant angle on flow structures and pollutant dispersion in the wake of the studied model vehicle. Int. J. Heat Mass Transfer 51 (25–26), 6180–6193.

Clifford, M.J., Clarke, R., Riffat, S.B., 1997. Local aspects of vehicular pollution. Atmos. Environ. 31 (2), 271–276.

Dong, G., Chan, T.L., 2006. Large eddy simulation of flow structures and pollutant dispersion in the near-wake region of a light-duty diesel vehicle. Atmos. Environ. 40 (6), 1104–1116.

Farell, C., Guven, O., Carrasquel, S., Patel, V.C., 1977. Effect of wind tunnel walls on the flow past circular cylinders and cooling tower models. J. Fluid Eng. – T. ASME 99 (4), 470–479.

Gosse, K., Paranthoen, P., Patte-Rouland, B., Gonzalez, M., 2006a. Dispersion in the near wake of idealized car model. Int. J. Heat Mass Transfer 49 (9–10), 1747–1752.

Gosse, K., Patte-Rouland, B., Gonzalez, M., Paranthoen, P., 2006b. Scalar dispersion in the near wake of a simplified model car. Exp. Fluid 40 (1), 135–140.

Guilmineau, E., 2008. Computational study of flow around a simplified car body. J. Wind Eng. Ind. Aerod. 96 (6–7), 1207–1217.

Hackett, J.E., Williams, J.E., Baker, J.B., Wallis, S.B., 1987. On the influence of ground movement and wheel rotation in the test on modern car shapes. SAE Technical Paper 870245.

Kanda, I., Uehara, K., Yamao, Y., Yoshikakwa, Y., Morikawa, T., 2006a. A wind tunnel study on exhaust gas dispersion from road vehicles. Part II: Effect of vehicle queues. J. Wind Eng. Ind. Aerod. 94 (9), 659–673.

Kanda, I., Uehara, K., Yamao, Y., Yoshikakwa, Y., Morikawa, T., 2006b. A wind tunnel study on exhaust gas dispersion from road vehicles. Part I: Velocity and concentration fields behind single vehicles. J. Wind Eng. Ind. Aerod. 94 (9), 639–658.

Khalighi, B., Zhang, S., Koromilas, C., Balkanyi, S.R., Bernal, L.P., Iaccarino, G., Moin, P., 2001. Experimental and computational study of unsteady wake flow behind a bluff body with a drag reduction device. SAE Technical Paper 2001-01-1042.

Kozaka, E.O., Ozkan, G., Ozdemir, I.B., 2004. Turbulent structure of three-dimensional flow behind a model car. 1. Exposed to uniform approach flow. J. Turbulence 5, Art. No. N2, 22 pages.

Krajnovic S., Davidson L., 2004. Large eddy simulation of the flow around simplified car model. SAE Technical Paper 2004-01-0227.

Krajnovic, S., Davidson, L., 2005a. Flow around a simplified car. Part 1: Large eddy simulation. J. Fluid Eng. 127 (5), 907–918.

Krajnovic, S., Davidson, L., 2005b. Flow around a simplified car. Part 2: Understanding the flow. J. Fluid Eng. 127 (5), 919–928.

Krajnovic, S., Davidson, L., 2005c. Influence of floor motion in wind tunnels on the aerodynamics of road vehicles. J. Wind Eng. Ind. Aerod. 93 (9), 677–696.

Lajos, T., Preszler, L., Finta, L., 1986. Effect of moving ground simulation on the flow past bus models. J. Wind Eng. Ind. Aerod. 22 (2–3), 271–277.

Lienhart, H., Becker, S., 2003. Flow and turbulent structure in the wake of a simplified car model. SAE Technical Paper 2003-01-0656.

Narasimha, R., Prasad, S.N., 1994. Leading edge shape for flat plate boundary layer studies. Exp. Fluid 17 (5), 358–360.

Vino, G., Watkins, S., Mousley, P., 2003. The passenger vehicle wake under the influence of upstream turbulence. SAE Technical Paper 2003-01-0650.

Watkins, S., Vino, G., 2008. The effect of vehicle spacing on the aerodynamics of a representative car shape. J. Wind Eng. Ind. Aerod. 96 (6–7), 1232–1239.